Controlled-source elastic interferometric imaging by multi-dimensional deconvolution with downhole receivers below a complex overburden

Joost van der Neut[1], Kurang Mehta[2], Jan Thorbecke[1] and Kees Wapenaar[1]*
[1]*Delft University of Technology, Department of Geotechnology, Delft, the Netherlands.*
[2]*Shell International E&P, Bellaire Technology Center, Houston, TX.*

Summary
Recently, various cross-correlation based methods have emerged to redatum source locations from the earth's surface to downhole receiver locations. By placing receivers in a horizontal or deviated well below a complex overburden and turning them into virtual sources, accurate imaging can be obtained without requiring a velocity model of the near subsurface. The underlying theory is based on the assumption that illumination is isotropic at the virtual source location. If this assumption is not fulfilled, virtual sources can be de-focused, spurious artifacts can enter the retrieved gathers and true amplitudes are generally not preserved. One way to correct for de-focusing is to replace cross-correlation with multi-dimensional deconvolution. This procedure is more involved and instabilities can occur during the required matrix inversions. We show that if elastic multi-dimensional deconvolution is followed by migration, many artifacts from instable inversion interfere destructively and well focused images can be obtained.

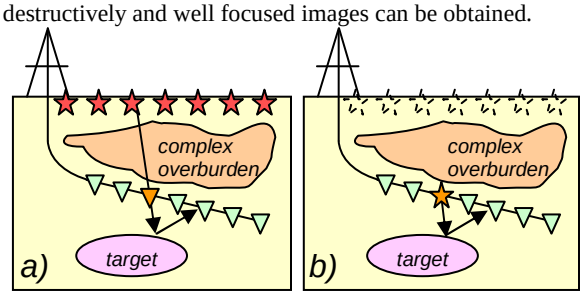

Figure 1: a) Input data with sources at the earth's surface and receivers placed in a well below a complex overburden but above the imaging target; b) Output data with virtual sources and receivers in the well.

Acoustic interferometry by cross-correlation
The virtual source method is an attractive technique for seismic imaging below a complex overburden (Bakulin and Calvert, 2006). The method requires the installation of receivers in horizontal or deviated wells below the major complexities that hamper conventional imaging from the earth's surface. Sources are located at the earth's surface, but are redatumed to the receiver level by a cross-correlation procedure. Input and output of this operation are illustrated in Figure 1a and 1b, respectively. The virtual source method is fully data-driven, meaning that no velocity model is required. Various related methodologies have emerged under the name of seismic interferometry (Schuster, 2001; Curtis et al., 2006; Wapenaar et al., 2008b, Schuster, 2009). Alternative applications have been presented, such as virtual crosswell imaging (Minato et al., 2007; Mehta et al., 2010) and interferometric salt flank imaging (Hornby and Yu, 2007; Vasconcelos et al., 2008; Lu et al., 2009; Ferrandis et al., 2009). Many of these methods can be represented by the following expression in the frequency-space (FX) domain:

$$\hat{C}(\mathbf{x}_B,\mathbf{x}_A,\omega)=\int_{\partial\mathbb{S}_{src}} W(\mathbf{x}_S)\hat{U}(\mathbf{x}_B,\mathbf{x}_S,\omega)\left\{\hat{V}(\mathbf{x}_A,\mathbf{x}_S,\omega)\right\}^{*} d\mathbf{x}_S . \quad (1)$$

The hat above the symbols denotes their presence in the FX-domain. $\hat{U}(\mathbf{x}_B,\mathbf{x}_S,\omega)$ is the recorded data at receiver $\mathbf{x}_B$ and $\hat{V}(\mathbf{x}_A,\mathbf{x}_S,\omega)$ is the recorded data at receiver $\mathbf{x}_A$, both due to a source at $\mathbf{x}_S$ evaluated at angular frequency ω. The integral is over the source array $\partial\mathbb{S}_{src}$. $W(\mathbf{x}_S)$ is an optional weighing function to taper the edges of the source array (Mehta et al., 2008). On the left-hand-side we find the cross-correlation function $\hat{C}(\mathbf{x}_B,\mathbf{x}_A,\omega)$. If the medium is lossless and sources are distributed regularly with sufficient aperture, $\hat{C}(\mathbf{x}_B,\mathbf{x}_A,\omega)$ can be interpreted as a scaled impulse response as if there was a virtual source at $\mathbf{x}_A$ and a receiver at $\mathbf{x}_B$, convolved with the auto-correlated source spectrum $|\hat{S}(\omega)|^2$. What $\hat{U}$ and $\hat{V}$ represent exactly depends on the type of interferometry that is applied. One option is to use full fields for both $\hat{U}$ and $\hat{V}$, as discussed by Wapenaar and Fokkema (2006). However, to retrieve a full Green's function, sufficient scattering should take place below the receivers (Wapenaar, 2006). If such conditions are not fulfilled, spurious artifacts can enter the retrieved responses (Snieder et al., 2006). This problem can partly be mitigated by choosing for $\hat{V}$ the time-gated direct field, as in the virtual source method of Bakulin and Calvert (2006). Alternatively, $\hat{V}$ can be the incident field and $\hat{U}$ the scattered field in a perturbation-based approach (Vasconcelos et al., 2009). $\hat{V}$ and $\hat{U}$ can also represent downgoing and upgoing wavefields (Mehta et al., 2007). The interpretation of the retrieved cross-correlation function depends on the choices made for $\hat{V}$ and $\hat{U}$. See Schuster and Zhou (2006) and Vasconcelos et al. (2008) for an overview of other options.

Controlled-source elastic interferometric imaging by multi-dimensional deconvolution with downhole receivers below complex overburden

Interferometry by cross-correlation has a lot in common with model-driven redatuming (Berryhill, 1979) as pointed out by Schuster and Zhou (2006) and Thorbecke and Wapenaar (2007). However, the Green's functions for interferometry are directly measured by downhole receivers. This allows us to redatum the source field much more accurately than in any model-driven approach and to handle multiple scattering properly.

Elastic interferometry by cross-correlation

Equation 1 is derived from acoustic wave theory. Interferometry can also be applied to elastic wavefields. Bakulin et al. (2007) showed that virtual S-wave sources can be generated from wave conversions at the ocean floor. Xiao et al. (2006) use PS converted waves to delineate salt flanks. A fundamental theory for interferometry in elastic media has been derived by Wapenaar and Fokkema (2006). We recast their expressions as

$$\hat{C}_{p,q}(\mathbf{x}_B,\mathbf{x}_A,\omega) = \int_{\partial\mathbb{S}_{src}} W(\mathbf{x}_S)\hat{U}_{p,k}(\mathbf{x}_B,\mathbf{x}_S,\omega)\left\{\hat{V}_{q,k}(\mathbf{x}_A,\mathbf{x}_S,\omega)\right\}^{*} d\mathbf{x}_S, \quad (2)$$

where Einstein's summation convention has been adopted, meaning that repeated index k is implicitly summed over. Symbols are similar as in equation 1, but subscripts are added to distinguish the various wavefield components. The exact meaning of $\hat{U}_{p,k}$ and $\hat{V}_{q,k}$ depends on the type of interferometry that is applied. $\hat{U}_{p,k}$ and $\hat{V}_{q,k}$ can refer to the p- and q-component of the full particle velocity field due to decomposed P- or S-wave sources (denoted by subscript k), as derived by Wapenaar and Fokkema (2006). Gaiser and Vasconcelos (2008) derived similar expressions with $\hat{U}_{p,k}$ and $\hat{V}_{q,k}$ being scattered and incident fields, respectively. Wavefields can also be decomposed at the receiver side prior to cross-correlation. In the expressions of Van der Neut and Wapenaar (2009), $\hat{U}_{p,k}$ and $\hat{V}_{q,k}$ represent downgoing and upgoing P- or S-wavefields from decomposed P- or S-wave sources. The interpretation of $\hat{C}_{p,q}$ varies according to the type of fields that are correlated.

Elastic interferometry by multi-dimensional deconvolution

We mentioned before that interferometry by cross-correlation is based on a set of assumptions. Firstly, the medium is assumed to be lossless. Secondly, the illumination conditions at the receiver location are assumed to be isotropic. Not properly fulfilling these conditions can lead to the retrieval of inaccurate responses and spurious events. To diagnose and improve virtual source characteristics, it can be helpful to interpret redatuming as an inversion problem. Instead of evaluating an integral over sources, we can also derive an integral over the downhole receiver array $\partial\mathbb{S}_{rec}$, as proposed by Wapenaar et al. (2008a). This can be done for either acoustic or elastic wavefields. We do the latter and cast the expressions in the following general form:

$$\hat{U}_{p,k}(\mathbf{x}_B,\mathbf{x}_S,\omega) = \int_{\partial\mathbb{S}_{rec}} \hat{D}_{p,q}(\mathbf{x}_B,\mathbf{x}_A,\omega)\hat{V}_{q,k}(\mathbf{x}_A,\mathbf{x}_S,\omega)d\mathbf{x}_A. \quad (3)$$

Once more, $\hat{V}_{q,k}(\mathbf{x}_A,\mathbf{x}_S,\omega)$ and $\hat{U}_{p,k}(\mathbf{x}_B,\mathbf{x}_S,\omega)$ are the wavefields at receivers $\mathbf{x}_A$ and $\mathbf{x}_B$ due to sources at $\mathbf{x}_S$. Note however that the integral is over receiver locations and the unknown deconvolution function $\hat{D}_{p,q}$ is part of the integrand and has to be solved by least-squares inversion. What $\hat{V}_{q,k}$ and $\hat{U}_{p,k}$ represent exactly, depends on the type of interferometry that is applied. Following Wapenaar et al. (2008a), $\hat{V}_{q,k}$ is the downgoing P- or S-wave field of a k-component source and $\hat{U}_{p,k}$ is the upgoing P- or S-wavefield of that same source component. As a consequence of this choice, the deconvolution function $\hat{D}_{p,q}$ can be interpreted as a scaled (bandlimited) impulse response as if there was a virtual source at $\mathbf{x}_A$, radiating in a medium in which all heterogeneities above the receiver array have been removed. This interesting advantage of multi-dimensional deconvolution proved useful for removing multiples from Ocean Bottom Cable recordings (Holvik and Amundsen, 2005). Note that multi-dimensional deconvolution requires multi-component receivers. If these are not available, approximate expressions can be derived with time-gated fields (van der Neut, 2009). It should be noted that the latter approach can not remove all overburden interactions, but can improve virtual source focusing. Inverting equation 3 in a least-squares sense is equivalent to solving the following normal equation, which can be obtained by cross-correlating both sides of equation 2 with $\hat{V}_{q',k}(\mathbf{x}'_A,\mathbf{x}_S,\omega)$, where $\mathbf{x}'_A$ is another receiver location, and integrating over $\mathbf{x}_S$, yielding

$$\hat{C}_{p,q'}(\mathbf{x}_B,\mathbf{x}'_A,\omega) = \int_{\partial\mathbb{S}_{rec}} \hat{D}_{p,q}(\mathbf{x}_B,\mathbf{x}_A,\omega)\hat{\Gamma}_{q,q'}(\mathbf{x}_A,\mathbf{x}'_A,\omega)d\mathbf{x}_A. \quad (4)$$

$\hat{C}_{p,q}$ is the cross-correlation function that we defined in equation 2. $\hat{\Gamma}_{q,q'}$ is defined as the illumination function:

$$\hat{\Gamma}_{q,q'}(\mathbf{x}_A, \mathbf{x}'_A, \omega) = \int_{\partial\mathbb{S}_{src}} W(\mathbf{x}_S)\hat{V}_{q,k}(\mathbf{x}_A, \mathbf{x}_S, \omega)\hat{V}^*_{q',k}(\mathbf{x}'_A, \mathbf{x}_S, \omega)d\mathbf{x}_S \quad (5)$$

Briefly said, the illumination function quantifies the de-focusing effect between locations $\mathbf{x}_A$ and $\mathbf{x}'_A$. If illumination is isotropic, $\hat{\Gamma}_{q,q'}$ converges to a bandlimited delta-function, as illustrated numerically by van der Neut and Thorbecke (2009). If illumination is not isotropic, then $\hat{C}_{p,q} \neq \hat{D}_{p,q}$, meaning effectively that virtual source data by cross-correlation is de-focused. Such de-focusing can be diagnosed directly by studying the illumination function. Virtual source focusing can also be improved by obtaining the inverse of the illumination function $\hat{\Gamma}^{inv}_{q',q}$ and applying this as a filter to the cross-correlation data, according to

$$\hat{D}_{p,q}(\mathbf{x}_B, \mathbf{x}_A, \omega) = \int_{\partial\mathbb{S}_{rec}} \hat{C}_{p,q'}(\mathbf{x}_B, \mathbf{x}'_A, \omega)\hat{\Gamma}^{inv}_{q',q}(\mathbf{x}'_A, \mathbf{x}_A, \omega)d\mathbf{x}'_A, \quad (6)$$

Equation 6 can be interpreted as Multi-Dimensional Deconvolution (MDD) (Wapenaar et al., 2008a). Under a layered medium approximation, MDD can be implemented in the frequency-wavenumber (FK)-domain, as demonstrated for acoustic media by van der Neut and Bakulin (2009). In laterally varying media, MDD can be implemented in the FX-domain (van der Neut et al., 2009). MDD has also applications for virtual crosswell data (Minato et al., 2009), Controlled Source Electromagnetic exploration (Fan et al., 2009; Hunziker et al., 2009), Ground Penatrating Radar (Kuroda and Slob, 2009), passive seismics (Wapenaar et al., 2008c) and lithospheric-scale imaging (Ruigrok et al., 2010).

The illumination function has a lot in common with the Point-Spread Function (PSF, or spatial resolution function) in seismic migration (Miller et al., 1987; Schuster and Hu, 2000; van Veldhuizen et al., 2008), being defined as the migration result of the response of a single point scatterer. As such, MDD can be compared with migration deconvolution, as often applied in imaging to improve the spatial resolution (Hu et al., 2001; Yu et al., 2006). However, the illumination function is obtained from measured responses, whereas the PSF is modeled in a smoothened background medium. As a consequence, the illumination function can account for multiple scattering much more accurately.

Synthetic example

In the following example, we apply interferometry to redatum multi-component sources from the earth's surface to multi-component receiver locations in a deviated well below a complex overburden. The data are obtained from a 2D elastic finite difference code, with a 60Hz source peak frequency. The elastic model is a 2D slice taken from a 3D synthetic model that is inspired by a real field of Shell in the Middle East (Korneev et al., 2009). We place 220 2-component force sources just below the earth's surface, covering an array of 657m, with 3m source spacing. The first 20 and last 20 source positions are tapered with a Hanning filter to reduce finite-array artifacts (Mehta et al., 2008). 128 multi-component receivers are located in a deviated well, with a spacing of 3.0852m, covering an array of ~392m, recording particle velocity and pressure. Below the well we find the fine layered structure that we aim to image. Both well and the target reflectors have a dip of ~15 degrees with respect to the earth's surface. See Figure 2a for an illustration. Due to the strong variations in medium properties in the near subsurface, the downhole wavefields are heavily distorted. The data are rotated to a Cartesian coordinate system with the horizontal and vertical axis parallel and perpendicular to the well, respectively, where the origin is chosen in the first receiver location. Full elastic decomposition requires knowledge of both the particle velocity and traction fields (Wapenaar and Berkhout, 1989). Since shear traction is not recorded, we derived an alternative flux-normalized decomposition scheme in the FK-domain where up- and downgoing S-waves are separated manually with an additional time-gate (van der Neut et al., 2010). As a result, particular multiple scattered S-waves and converted wave modes have not been handled correctly, which does not seem to harm our analysis. Due to their relatively short wavelength at 60Hz, S-waves proved more useful for imaging the fine layered structure below the well than P-waves. That's why we focus our attention to the retrieved SS reflection response. In Figure 2b we show the zero-offset S-wave reflectivity in the rotated medium below the receivers, derived directly from the velocity model. We aim to produce a bandlimited image of this reflectivity, using seismic interferometry followed by a one way wave equation based migration code (Thorbecke, 1997). This migration is performed in a reference medium, where all heterogeneities above the well have been removed, such that we do not require a velocity model of the complex overburden. We created a reference response by placing multi-component active shots at all receiver locations and applying elastic decomposition at the source and receiver side in the FK-domain. Note that the medium properties are not exactly homogeneous at the receiver array, such that neither the reference response nor

Controlled-source elastic interferometric imaging by multi-dimensional deconvolution with downhole receivers below complex overburden

the redatumed data is exact. We picked a reference virtual source location at ~151m from the first receiver (#50). In Figure 3a we show a virtual shot record retrieved by cross-correlation (red) at this location, overlaid by the reference response (black). We find a relatively good match. In Figure 3b we show the result after migration, revealing indeed a bandlimited image of the S-wave reflectivity (Figure 2b). However, not all reflectors are clearly visible. To diagnose virtual source de-focusing, we show the S-wave illumination function of the reference virtual source in Figure 4a. Note that we find indeed a bandlimited delta function, smeared out in time and space. The illumination function is rewritten as a monochromatic matrix $\hat{\mathbf{\Gamma}}$ (Berkhout, 1982), hosting source locations and components as columns and receiver locations and components as rows. For each frequency component, matrix $\hat{\mathbf{\Gamma}}$ is inverted with a stabilization parameter ε, according to $\hat{\mathbf{\Gamma}}^{\mathrm{inv}} = \left[\hat{\mathbf{\Gamma}} + \varepsilon^2 \mathbf{I}\right]^{-1}$, where $\mathbf{I}$ is an identity matrix. This approach offers some freedom in the choice of ε. To improve virtual source focusing to the max, we choose ε relatively low (around 2% of the maximum of the matrix diagonal). To visualize the improved resolution, we convolved the illumination function with its stabilized inverse and plotted the result in Figure 4b. Note that the result is much closer to the desired bandlimited delta function. We use the inverted illumination function to filter the cross-correlation function (equation 6), a process that is equivalent to multi-dimensional deconvolution. In Figure 5a we show the reference virtual shot record after this operation. Note that improvements are hardly visible, due to the various inversion artifacts that populate the gather. However, after migrating these virtual shot gathers, many of these artifacts interfere destructively and we can still retrieve a relatively well-focused S-wave image – Figure 5b. Compared to Figure 3b we notice the improved resolution and the closer correlation with the true reflectivity (Figure 2b). At the downside, we find noise resulting from the instable inversion, which could be reduced by increasing ε, at the cost of losing resolution. In the limit $\varepsilon \to \infty$, multi-dimensional deconvolution converges back to cross-correlation. The optimal ε seems a matter of choice.

Conclusion

With interferometry we can turn downhole receivers into virtual sources. The methodology is similar to various model-driven approaches. However, with interferometry we make use of measured Green's functions without relying on a subsurface velocity model. Because of this, multiple scattering can be taken into account and very accurate redatuming can be achieved. As in model-driven redatuming, resolution can be improved by replacing cross-correlation with multi-dimensional deconvolution. Since measured Green's functions are adopted, very accurate focusing can be achieved without relying on a smoothed velocity model. We showed that artifacts emerging from instable matrix inversions are often interfering destructively if wavefield redatuming is followed by migration.

Acknowledgements

This work was supported by the Dutch Technology Foundation STW, applied science division of NWO and the Technology Program of the Ministry of Economic. We thank Shell E&P for permission to show the elastic model.

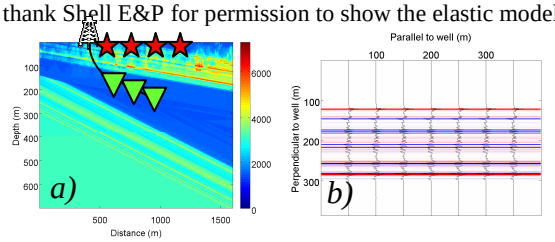

Figure 2: a) Configuration and shear impedances of the elastic model; b) Zero-offset S-wave reflectivity below the well, with the X-axis parallel to the well.

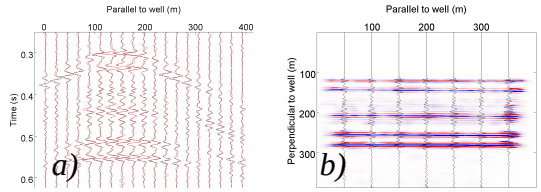

Figure 3: Interferometry by cross-correlation; a) Retrieved virtual shot record (red) overlaying the reference response (black); b) Migrated S-wave image.

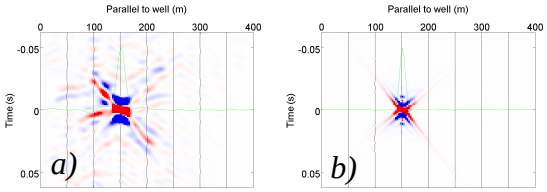

Figure 4: Illumination function at the reference virtual source location; a) by cross-correlation; b) after multi-dimensional deconvolution.

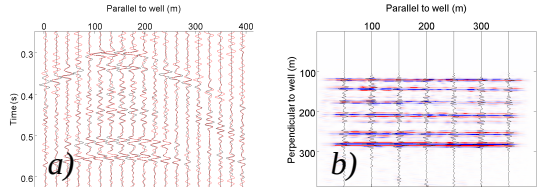

Figure 5: Interferometry by multi-dimensional deconvolution; a) Retrieved virtual shot record (red) overlaying the reference response (black); b) Migrated S-wave image.